Coastal Marine Science 30(1): 54–61, 2006

Numerical experiment on the sedimentation in Manila Bay

Wataru FUJI-IE[1] and Tetsuo YANAGI[2]*

[1] *Faculty of Environmental and Symbiotic Sciences, Prefectural University of Kumamoto, 3–1–100 Tsukide, Kumamoto 862–8502, Japan*
**E-mail: fujiie@pu-kumamoto.ac.jp*
[2] *Research Institute for Applied Mechanics, Kyushu University, 6–1 Kasuga-kouen, Kasuga, Fukuoka 816–8580, Japan*

Received: 10 October 2005; Accepted: 31 October 2005

Abstract—Sedimentation process of suspended matter in Manila Bay supplied from Pampanga River, Pasig River and open ocean is investigated using a three-dimensional numerical model which includes tidal current, residual flow and current due to wind waves. The calculation results well reproduced the major characteristics of the observed sedimentation patterns of silt and clay. The calculation results reveal that the seasonal variability of deposited clay distribution is larger than that of silt in Manila Bay. The area that cysts can accumulate is discussed with the use of the calculation results of clay.

Key words: Manila Bay, numerical experiment sedimentation process

Introduction

Manila Bay is located along the southwestern coast of Luzon Island (Fig. 1). It is one of the areas greatly affected by toxic algal blooms in the Philippines. For example, A *Pyrodinium bahamense var. compressum* bloom was firstly reported in 1988 and reocurred almost every year until 1998. The hypnozygote of *P. bahamense var. compressum* in the surface sediment is believed to germinate after a required dormancy period if environmental conditions would be favorable. These newly germinated cysts then serve as the initial vegetative population, which can increase and eventually develop into a bloom (Azanza et al. 2004). Therefore, areas with high cyst density may be the locations where blooms start and spread. The areas with high cyst density coincided with areas where sediment accretion is likely to occur in Manila Bay (Siringan and Ringor 1998). Therefore, it is important to investigate how suspended matters are deposited in the bay.

Azanza et al. (2004) reported the horizontal distributions of sand, silt and clay in the surface sediment of Manila Bay using observation data. However, no attempt has been made to clarify the sedimentation process of suspended matters in Manila Bay. In this study we carry out a numerical experiment in order to investigate the sedimentation process of silt and clay supplied from two major rivers (Pampanga and Pasig) and open ocean with the use of three-dimensional numerical model of Manila Bay which includes tidal current, tide-induced residual current, density-driven current, wind driven current and current due to wind waves.

Numerical Model

Current field in Manila Bay

Numerical model of currents in Manila Bay has been already established. Fuji-ie et al. (2002) well reproduced the tidal currents there with the use of a horizontally two-dimensional numerical model and they also calculate the tide-induced residual current. M_2, S_2, K_1, O_1 and M_4 tides are taken into consideration in their model. Calculated tidal currents are shown in Fig. 2. M_2 tidal current amplitude is about 15 $cm \cdot s^{-1}$ at the mouth of the bay. It flows crossing the mouth of the bay. Off Pampanga, it becomes about 10 $cm \cdot s^{-1}$. S_2 tidal current amplitude is about 5 $cm \cdot s^{-1}$ at the mouth of the bay and 5 $cm \cdot s^{-1}$ off Pampanga. M_4 tidal current amplitude is about 5 $cm \cdot s^{-1}$ at the mouth of the bay and becomes 5 $cm \cdot s^{-1}$ off Pampanga. K_1 tidal current is about 12.0 $cm \cdot s^{-1}$ at the mouth of the bay and 8.0 $cm \cdot s^{-1}$ off Pampanga. O_1 tidal current amplitude is about 10.0 $cm \cdot s^{-1}$ at the mouth of the bay and 9.0 $cm \cdot s^{-1}$ off Pampanga. M_2 tidal current is most dominant in the bay although K_1 (30 cm at Manila) and O_1 (28 cm at Manila) tidal amplitudes are larger than M_2 (19 cm at Manila). The reason is due to the shorter period of M_2 constituent than K_1 and O_1.

As for the residual current, it is given as a linear superposition of tide-induced residual current, wind-driven current and density-driven current in the coastal sea (Yanagi, 1999). Fuji-ie et al. (2002) investigated the seasonal variation of density-driven and wind-driven currents there with the use of a three-dimensional numerical model which included observed sea surface heat flux, river discharge and wind data. Figure 3 shows the average wind direction and speed from 1961 to 1995 at Manila. From February to May, wind direc-

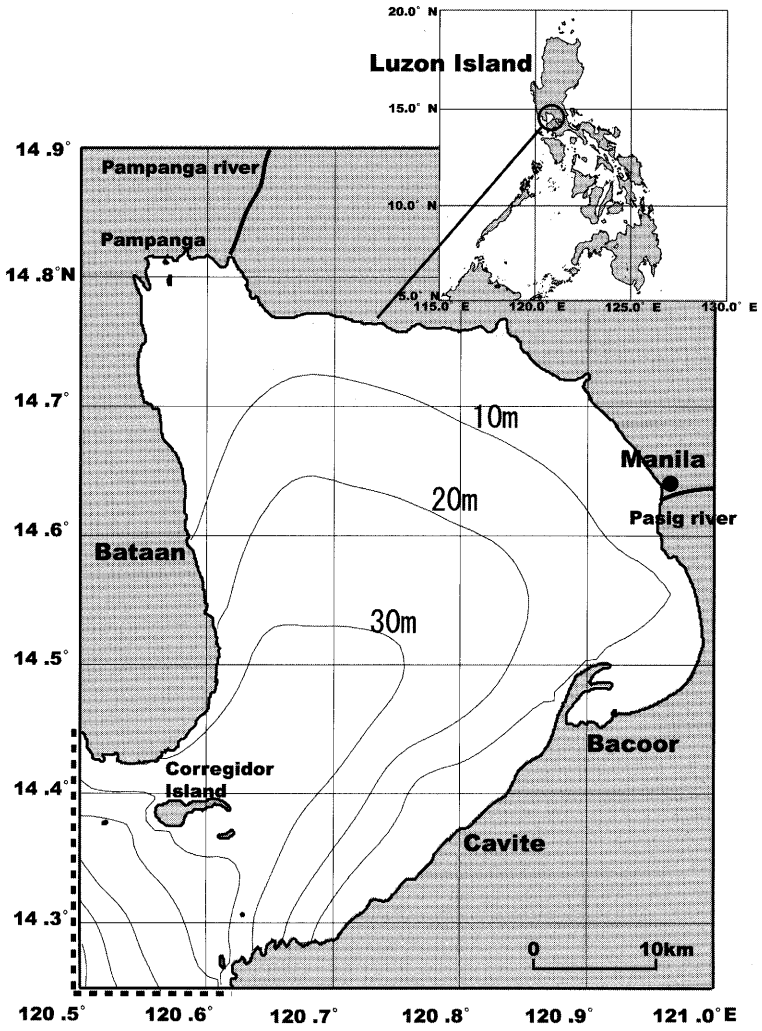

Fig. 1. Model area with bathymetry. Closed circle shows the tide gauge station. Broken line shows the open boundary of the numerical model, and thick lines show rivers flowing into Manila Bay.

tion is from southeast. From June to September, wind direction is from southwest. From November to January, wind direction is from northeast. Fuji-ie et al. (2002) calculated three types of wind-driven and density-driven currents during February to May, June to September and November to January.

Calculated tide-induced, wind-driven and density-driven currents in Manila Bay from February to May, from June to September and from November to January are shown in Fig. 4, respectively. Large variability is seen in residual current field. Although wind-driven current predominates in the surface layer, its direct influence is small in the middle and bottom layers. Residual currents flow along the wind direction in shallow areas. In the area with large depth, the compensated flow is dominant in the middle and bottom layers. Residual current speed is about $5\,\mathrm{cm}\cdot\mathrm{s}^{-1}$ above the bottom. We combined the results of tidal current and residual current into one three dimensional tracer model in this paper.

Water velocity amplitude due to wind waves is given by the following formula on basis of small amplitude wave theory (Tsubaki 1974);

$$U_{wave}=\frac{H_{wave}gT}{2L\cosh(2\pi H/L)}, \tag{1}$$

where U_{wave} denotes water velocity amplitude due to wind waves and H, H_{wave}, T and L are water depth, significant wave height, wave period and wave length, respectively. The significant wave length depends on the water depth and the significant wave period, and it is calculated as follows;

$$L=\frac{gT^2}{2}\tanh\left(2\left(\frac{H}{gT^2}\right)^{1/2}\left(1+\left(\frac{H}{gT^2}\right)^{1/2}\right)\right). \tag{2}$$

Wilson (1965) showed that the significant wave height and wave period are calculated by the following equation;

$$gH_{wave}/U_{wind}^2=0.3(1-(1+0.004(gF/U_{wind}^2)^{1/2})^{-2}), \tag{3}$$

$$gT/2\,\pi U_{wind}=1.37(1-(1+0.008(gF/U_{wind}^2)^{1/3})^{-5}), \tag{4}$$

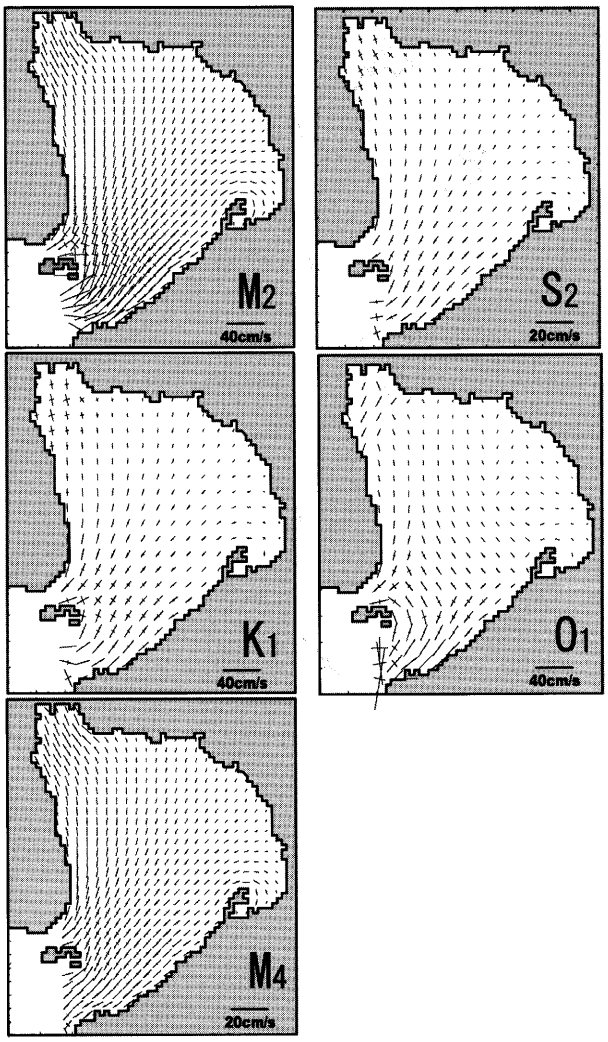

Fig. 2. Calculated long and short axes of M_2, S_2, K_1, O_1 and M_4 tidal current ellipses (Fuji-ie et al. 2002).

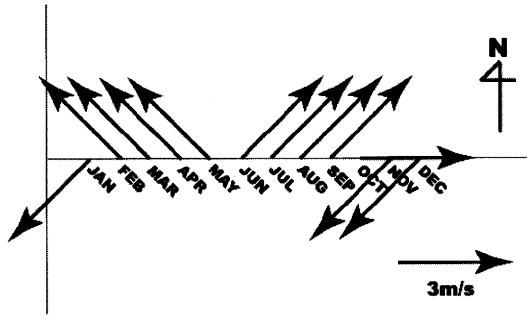

Fig. 3. Wind speed and direction at Manila (average in 1961–1995, Philippine Atmospheric, Geophysical and Astronomical Services Administration).

where F denotes the fetch length and U_{wind} is wind speed 10 m above the sea surface. Figure 5 shows the horizontal distributions of water velocity amplitude above the sea bottom due to wind waves under three different winds. Maximum water velocity amplitude due to wind waves throughout a year is about 4 $cm \cdot s^{-1}$ in Manila Bay. Water velocity amplitude due to wind waves is taken into consideration in this study.

Tracer model

Suspended matters supplied from rivers and open ocean are transported by tidal current and residual current, sink and settle at some points of the sea bottom. Some suspended matters deposit there and are buried but other suspended matters are resuspended and move again.

The Eular-Lagrange method is used to track the movement of a suspended matter in this numerical model. The position of suspended matter X_{n+1} $(x_{n+1}, y_{n+1}, z_{n+1})$ at time n+1, which was X_n (x_n, y_n, z_n) at time n, can be calculated by the following equation:

$$X_{n+1} = X_n + V\Delta t + \frac{1}{2}(\nabla V)V\Delta t^2 + w_s \Delta t + R, \qquad (5)$$

where V denotes the three-dimensional velocity vector; Δt, the time step; ∇, the horizontal gradient; w_s, the sinking velocity of suspended matter by the Stokes law;

$$W_s = -\frac{2g(\rho_p - \rho_w)}{9v} r^2, \qquad (6)$$

where g $(=980\,cm \cdot S^{-2})$ denotes the gravitational acceleration; ρ_p, the density of suspended matter; ρ_w, the density of sea water; v $(=0.0115\,cm \cdot S^{-2})$, the viscosity of sea water; r, the diameter of suspended matter. R is the dispersion due to the turbulence and is given by the following equation,

$$R_x \text{ and } R_y = \gamma(2\Delta t D_h)^{1/2}, \qquad (7)$$

$$R_z = \gamma(2\Delta t D_v)^{1/2}, \qquad (8)$$

where γ is the normal random number whose average is zero and D_v whose standard deviation is 1.0. D_h and are the horizontal and vertical dispersion coefficients and they depend on the M_2 tidal current amplitude as follows;

$$D_h = 3000 \times V_{amp}^2, \qquad (9)$$

$$D_v = 0.015 \times V_{amp}^2, \qquad (10)$$

Here V_{amp} denotes the amplitude of M_2 tidal current (Yanagi and Inoue 1995).

When a suspended matter reaches the sea bottom, we judge whether it stops moving or removes by applying the critical tractive force theory (Tsubaki 1974);

$$F = \frac{\rho_W}{2} C_t U_b^2 \frac{\pi}{4} r^2, \qquad (11)$$

$$R = \frac{\pi}{6} r^3 (\rho_p - \rho_w) C_s g, \qquad (12)$$

where F denotes the tractive force; R, the resistance force; C_t $(=0.4)$, the drag coefficient of suspended matter; C_s $(=1.0)$,

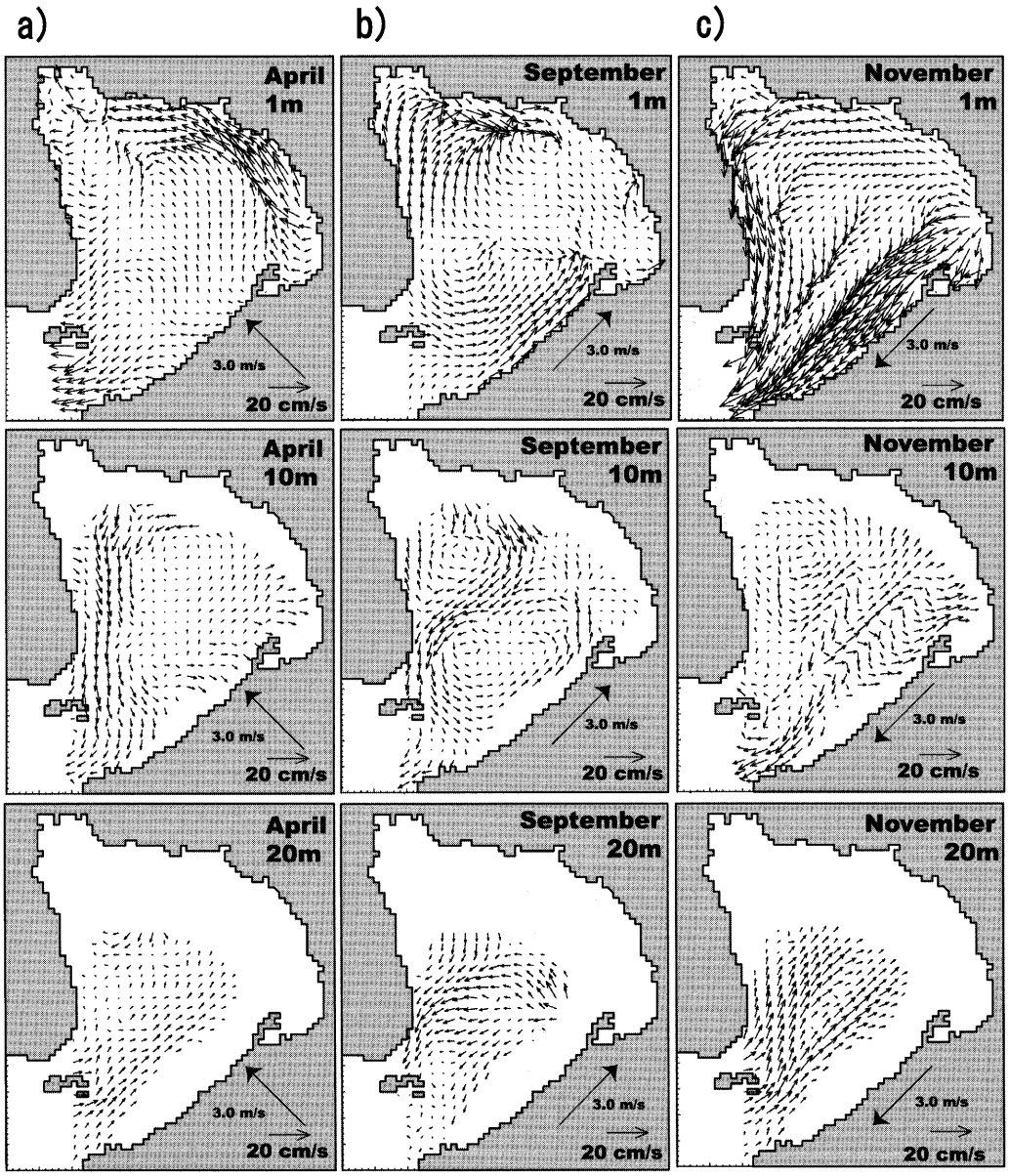

Fig. 4. Calculation results of residual currents from February to May (a), from June to September (b) and from November to January (c). Thick arrow represents wind direction (Fuji-ie et al. 2002).

the static friction coefficient of suspended matter; U_b, the velocity just above the sea bottom. We assume that the velocity just above the sea bottom is 0.1 times the calculated velocity in the lowest layer of the numerical model and it is given by the following formula;

$$U_b = 0.1 \times (U_t + U_r \cos B) + U_{wave}, \quad (13)$$

where U_t denotes the calculated M_2 tidal current amplitude; U_r, the calculated residual current velocity; B, the angle between the long axis of tidal current and the direction of residual currrent.

When R is larger than F, a suspended matter stops moving and deposits at the position where the suspended matter settles and when F is larger than R, it removes from its position. When the suspended matter crosses the open boundary of this model we pick it up.

Azanza et al. (2004) reported the horizontal distributions of sand, silt and clay in the surface sediment of Manila Bay using observation data. The modal diameter of observed deposited sand is 0.375 mm. Since the critical tractive velocity of the sand (more than 13 $cm \cdot s^{-1}$) is faster than the current speed above the sea bottom in Manila Bay, the sand in Manila Bay can not be transported by the ordinary current, that is, tidal current and residual current. It is likely that the deposited sand in a wide area of Manila Bay were transported by storms. Therefore, only silt and clay sedimentation process is investigated in this study.

On the basis of the observation results by Azanza et al. (2004), two kinds of particles (silt and clay) are injected from two major rivers and open ocean in this model. Silt particles

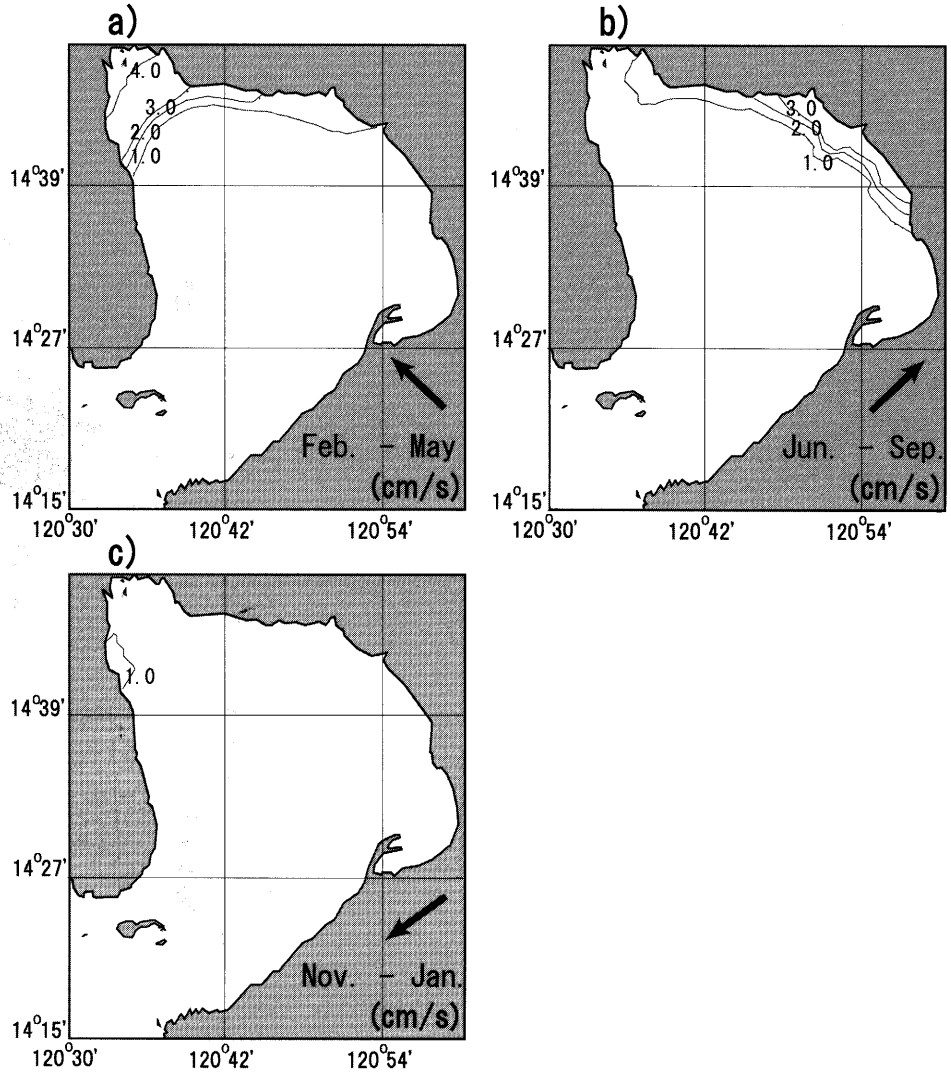

Fig. 5. Horizontal distribution of water velocity amplitude above the bottom due to wind waves in Manila Bay from February to May (a), from June to September (b) and from November to January (c). Contour interval is 1.0 cm·s^{-1}. Thick arrow shows wind direction at Manila.

with the modal grain size of 0.016 mm and clay particles with the modal grain size of 0.001 mm are injected. These particles have the same density, that is, the density of 2.5 g·cm^{-3}. 500 particles are arranged every 1 m at the mesh of injection points of Manila Bay. Injection depth is 1 m in Pampanga River and Pasig River and is 1 m above the sea bottom along the open boundary of this model which is shown by broken line in Fig.1.

Results and Discussion

The calculated horizontal distributions of deposited silt and clay in different seasons are shown in Fig. 6. Silt deposits at the mouth of Manila Bay, near Manila and Pampanga Bay in all seasons. Clay deposits at the center of Manila Bay and near Manila in all seasons. The accumulated number of clay particles increases near Manila and decrease at the center of the bay in November to January. This is due to that the residual currents flow toward the head of the bay in the middle and bottom layers from November to January. Therefore, the small particles are transported to the head of Manila Bay.

In comparison with the seasonal variability of deposited silt distribution, the variability of deposited clay is large in Manila Bay. This result is explained by the critical tractive force theory. The comparisons of the tractive force and the resistance force for silt and clay in different seasons are shown in Fig. 7. Shadow region represents the area where the resistance force is larger than the tractive force. Seasonal variability of the shadow area of silt is large near the mouth and the head of Manila Bay. In contrast, the seasonal variability of clay is complex in Manila Bay. The seasonal variability of deposited clay distribution is larger than that of silt,

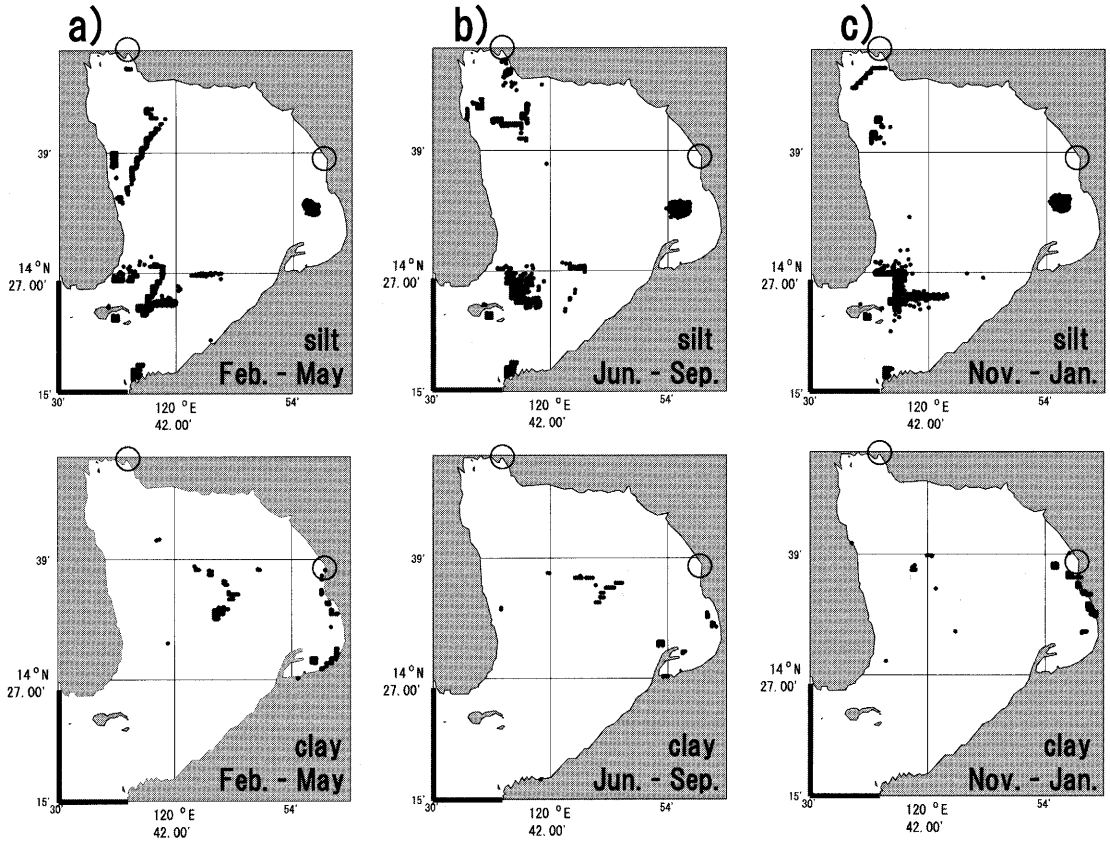

Fig. 6. Calculated horizontal distributions of deposited silt and clay from February to May (a), from June to September (b) and from November to January (c). Open circles and thick line denote the injection points. Black circles represent accumulated particles.

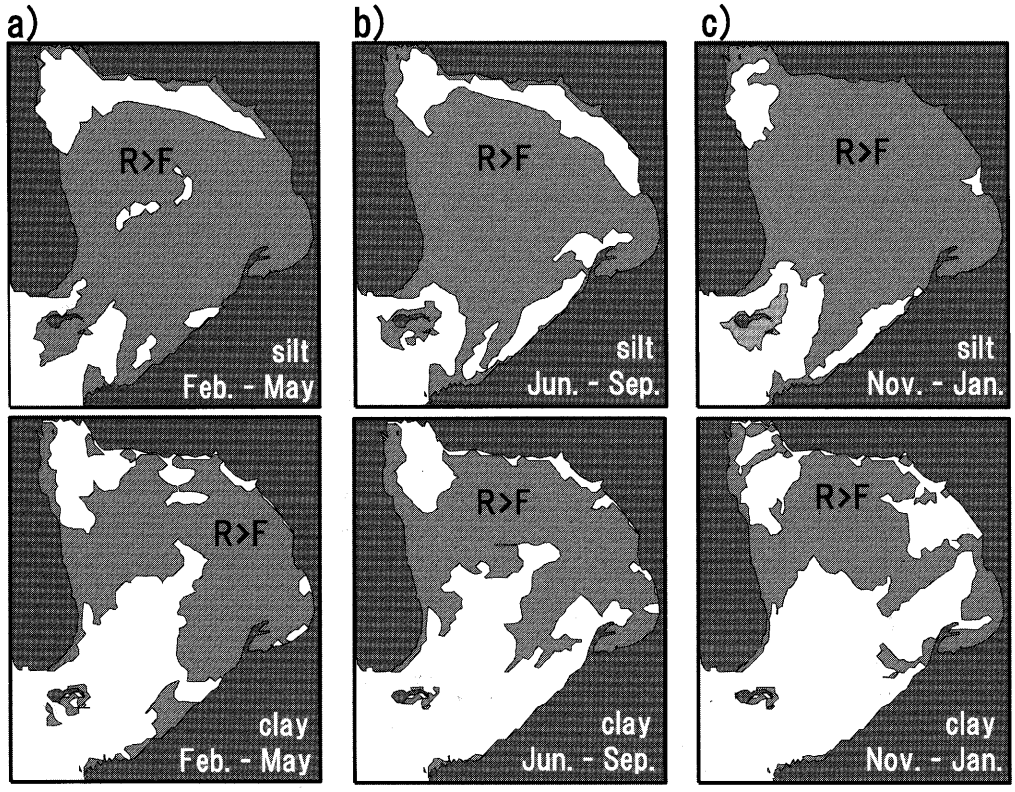

Fig. 7. Comparison of tractive and resistance forces from February to May (a), June to September (b) and November to January (c), respectively. Shadow region shows the area where the resistance force is larger than the tractive force and white area the opposite case.

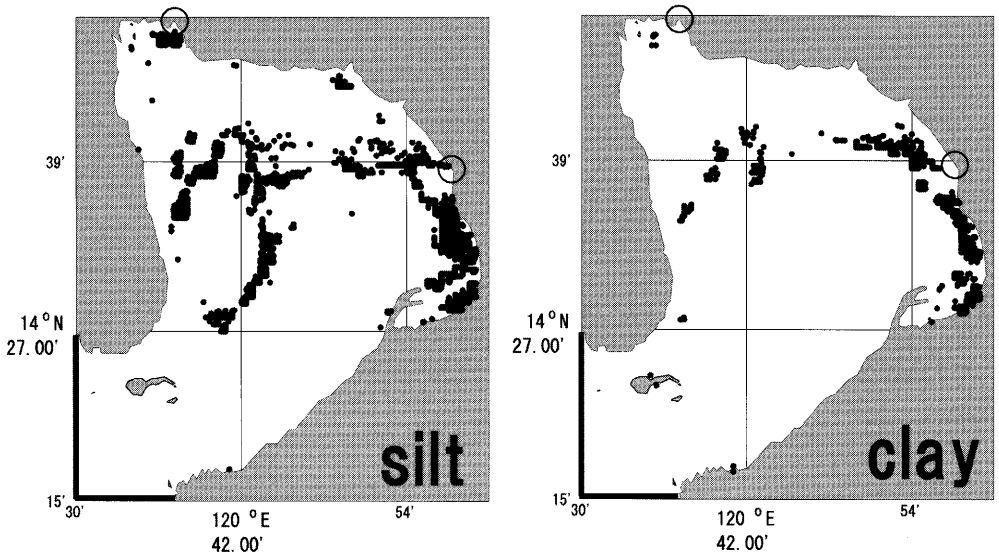

Fig. 8. Horizontal distributions of deposited silt and clay throughout the year in Manila Bay. Open circles and thick line denote the injection points. Black circles represent accumulated particles.

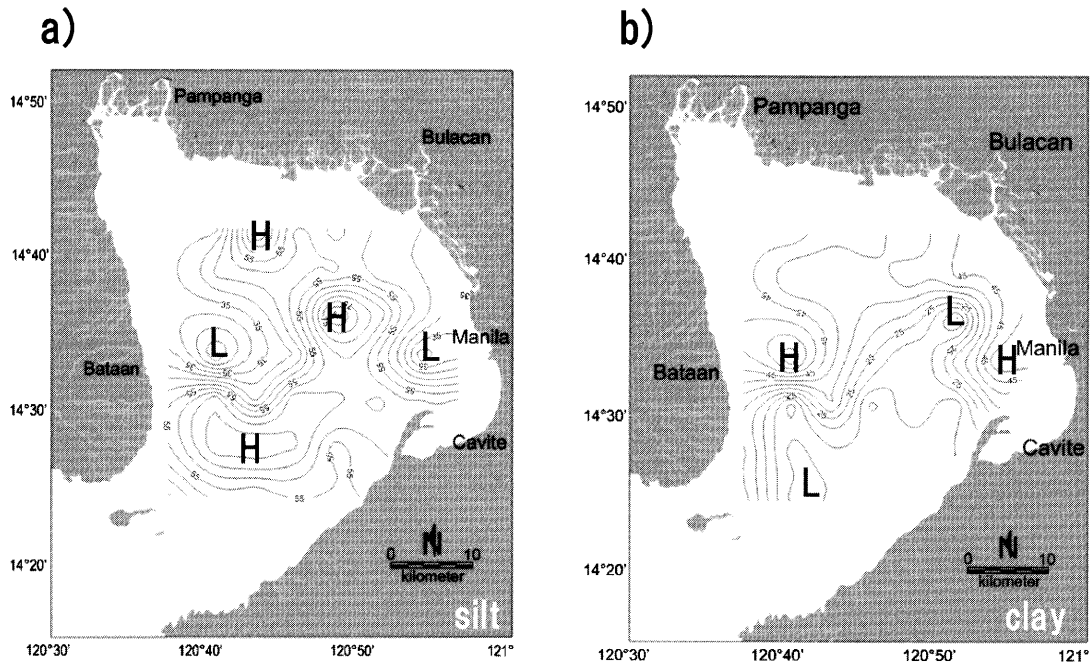

Fig. 9. Observed horizontal distributions of the particle fraction of surface bottom silt (a) and clay (b) in Manila Bay by Azanza et al. (2004).

because the seasonal variability of the shadow region about clay is larger than that about silt.

The calculated horizontal distributions of deposited silt and clay throughout the year, which were obtained by the tracer calculation being began in February and ended in January, are shown in Fig. 8. Silt is concentrated in the western part of Manila Bay and extends towards the center of the bay, that is, Pampanga Bay and coastal area of Manila. Clay is deposited in the western part of Manila Bay, Pampanga Bay and near Manila. The observed horizontal distributions of the particle fraction of surface sediment in Manila Bay are shown in Fig. 9 (Azanza et al. 2004). Silt is concentrated in the northwestern and southwestern parts of Manila Bay and extends towards the central part of the bay (Fig. 9a). The calculated regions of deposited silt roughly reproduce the observed silt region shown in Fig. 9 except near Manila. Observed clay concentration is high in the western part of Manila Bay and near Manila (Fig. 9b). The calculated horizontal distribution of deposited clay also roughly reproduces the observed clay region shown in (Fig. 9b). Such results suggest that our numerical experiment is qualitatively reliable in Manila Bay.

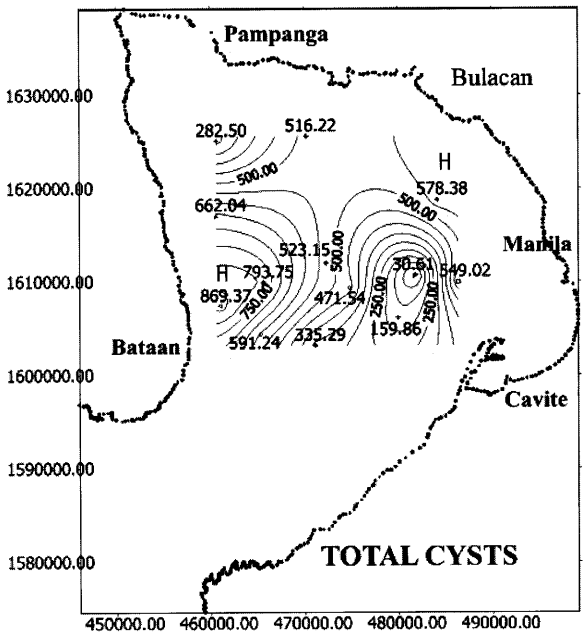

Fig. 10. Observed spatial distribution of total cysts in the surface sediment by Azanza et al. (2004). Unit is cysts·cm^{-3}.

Azanza et al. (2004) claimed that high cyst density is generally high in the area where clay content is high. Turgeon et al. (1990) reported that cyst with no motility is affected by the current as well as the sedimentation process similar to that of other suspended matters. Of course, there is a difference in the sedimentation processes of cyst and clay because the densities of cyst and clay are different. It is difficult at the present stage to calculate the sedimentation process of cyst because the density of cyst, the behavior characteristics of cyst are not clarified yet. Additionally, it is difficult to reproduce the sedimentation process of cyst by using the numerical model because the process by which a vegetative cell becomes a cyst is not clarified yet. In this paper we limit the discussion on the area that cysts can accumulate with the use of the calculation results of clay.

Figure 10 shows the observed spatial distribution of total cysts (Azanza et al. 2004). High concentration areas of the total cysts exist in the western part of Manila Bay and near Manila. The pattern of high concentration areas of the total cysts is similar to that of clay shown in (Fig. 9b). The concentration of total cysts becomes small in the southeastern part of Manila Bay and Pampanga Bay, as represented in Fig. 10. The reason for this pattern is explained by the critical tractive force theory as follows. Toxic algal blooms usually appear in Manila Bay from June to August (Ferida et al. 1996). The lower picture in (Fig. 7b) shows that clay cannot accumulate in the southeastern part of Manila Bay and Pampanga Bay from June to September. Cyst which sinks in the southeastern part of Manila Bay and Pampanga Bay is resuspended and is transported by the bottom current and deposited in the area where the resistance force is larger than the tractive force. Cysts cannot accumulate in the area where the algal blooms occur when the tractive force is larger than the resistance force there. The accumulated number of deposited cysts in the southwestern part of Manila Bay is larger than that near Manila. Cysts can accumulate in the southwestern part of Manila Bay and near Manila from June to August because the resistance force is larger than the tractive force in both areas (Fig. 7b).

Conclusion

This study revealed the sedimentation process of suspended matters in Manila Bay. One of the future direction of this study is to clarify the transport and sedimentation processes of cysts after the toxic algal bloom in Manila Bay. It will be very useful to understand the generation mechanism of toxic algal bloom in Manila Bay.

References

Azanza, R. V., Shringan, F. P., Sandiego-Mcglone, M. L., Yinguez, A. T., Macalalad, N. H., Zamora, P. B., Agustin, M. B. and Matsuoka, K. 2004. Horizontal dinoflagellate cyst distribution, sediment characteristicsand benthic flux in Manila Bay, Philippines. Phycological Res. 52: 376–386.

Bajarias, F. F. A. and Juan, R. R. Jr. 1996. Hydrological and climatological parameters associated with the Pyrodinium blooms in Manila Bay, Philippines. Harmful and Toxic Algal Blooms, Yasumoto, T., Oshima, Y and Fukuyo, Y. (ed.), pp. 49–52, Intergovermental Oceanographic Commission of UNESCO.

Fuji-ie, W., Yanagi, T. and Shiringan, F. P. 2002. Tide, tidal current and sediment transport in Manila Bay. La mer 40: 137–145.

Siringan, F. P. and Ringor. L. 1998. Changes in bathymetry and their implicationsto sediment dispersal and rates of sedimentation in Manila Bay. Sci. Diliman 2: 12–26.

Tsubaki, T. 1974. Hydraulics 2. Morikita Press, Tokyo, 216 pp. (in Japanese).

Turgeon, J., Cembella, A. D., Therriault, J.-C. and Beland, P. 1990. Spatial distribution of resting cysts of Alxandrium spp. In sediments of the lower St, Lawrence estuary and the Gaspe coast (eastern Canada), in "Toxic marine phytoplankton", Graneli, E., B. Sundstrom, L. Edler, and D. M. Anderson. (ed.), pp. 238–243, Elsevier, New York.

Wilson, B. W. 1965. Numerical prediction of ocean waves in the North Atlantic for December, 1959. Deut. Hydrogr. Zeit, Jahrgang 18 Heft 3: 114–130.

Yanagi, T. 1999. Coastal Oceanography. Kluwer Academic Publisher, Dordrecht, 162 pp.

Yanagi, T. and Inoue, K. 1995. A numerical experiment on sedimentation processes in the Yellow Sea and the East China Sea. J. Oceanogr. 51: 537–552.